Effect of the thickness on the mixed mode crack front fields

Shafique M.A. Khan*

*Department of Mechanical Engineering, King Fahd University of Petroleum and Minerals,
Dhahran, 31261, Saudi Arabia*

Abstract. Results pertaining to 3D investigations on the effect of the thickness on the stress fields at the crack front are presented. A 3D finite element analysis is performed using a modified single edge-notched tension specimen configuration, with an inclined crack to include mixed mode I-II. A technique to mesh the crack front (3D) with singular finite elements in ANSYS without using third party software is introduced and used in this study. The effect of the specimen thickness is explicitly investigated for six thicknesses ranging from 1 to 32 mm. In addition, three crack inclination angles, including pure Mode-I, are used to study the effect of mixed-mode I-II fracture. An attempt is made to correlate the extent of a particular stress state along the crack front to thickness. In addition, $\sigma_{zz}/\nu(\sigma_{xx} + \sigma_{yy})$ contours at the crack front are presented as a useful means to analyze the stress state.

Keywords: SENT; thickness; mixed mode; crack front mesh

1. Introduction

The crack tip fields and the nature of the crack-tip core regions are important factors in understanding and predicting fracture behavior of materials. Normally these crack tip fields are obtained assuming either a plane stress or plane strain condition at the crack tip. This approach delivers useful two-dimensional fields with reasonable accuracy. However, three-dimensional crack front fields are needed to fully understand the fracture process, which is the subject of this study. In addition, a new technique to mesh the crack front entirely in ANSYS environment is introduced for the considered geometry thus eliminating the need of third party software.

There have been various experimental studies to examine the crack-tip core region. Mishra and Parida (1985) studied the size of crack-tip core region in a thin sheet under pure Mode-I loading using photostress coating method. Jendoubi *et al*. (1991) and Ranganathan *et al*. (1994) presented experimental results on determination of shape and size of crack-tip strain fields using micro-strain gauges in compact tension specimen under cyclic loading. They presented isostrain contours and discussed plane stress and plane strain conditions. Kim *et al*. (2003) measured the magnitude of the plastic zone around the crack-tip and crack growth under cyclic loading. They used double edge-notched tension specimen and employed the Electronic Speckle Pattern Interferometry (ESPI)

---

*Corresponding author, Ph.D., E-mail: skhan@kfupm.edu.sa

system. They compared the observed crack-tip zones with that deduced through a finite element analysis and with the Irwin's estimate of the crack-tip plastic zone, and concluded that the experimental values lie between plane stress and plane strain states' values. Maccagno and Knott (1989) used the photoelastic technique to study the shape of the core region in a bend bar specimen of polymethylmethacrylate (PMMA) and captured the photoelastic pattern under pure Mode I, pure Mode II and mixed modes I-II for two different angles.

On the theoretical side, Theocaris and Andrianopoulos (1982) presented the Mises elastic boundary around the crack tip in addition to three other quantities, namely the strain-energy density factor, ratio of the dilatational to the distortional component of strain energy density, and the strain energy density around the crack tip. Banks and Garlick (1984) presented a summary and results for calculation of crack-tip plastic zone for pure Mode-I crack for both isotropic and anisotropic materials, considering both the plane stress and plane strain conditions at the crack tip. Khan and Khraisheh (2004) presented a detailed analysis of the crack-tip core regions for mixed mode I-II crack loading conditions. They considered both plane stress and plane strain conditions at the crack tip in addition to four different loading conditions for the cracked plate with a through thickness crack. Several researchers also investigated the 3D nature of the crack-tip fields. Wang *et al*. (1996) investigated shape and size of crack-tip zones using a constraint factor to introduce 3D effects. Nakamura and Parks (1988) performed 3D finite element analysis on a thin elastic plate to characterize the 3D stress state around a through-crack front under Mode I loading. They simulated a near crack front circular region around the crack front, while assuming a global behavior as Mode I plane stress and prescribing it to the outer boundary of the circular disk. They concluded that a strong 3D stress field exists within half-the-thickness distance from the crack front and at about 1.5 times the thickness, the stress state becomes essentially two-dimensional. They also concluded that Poisson's ratio has no effect on the extent of 3D effects. Nakamura and Parks (1989) also extended their study to pure Mode II crack by assuming a global Mode II plane stress loading and arrived at similar conclusions as that of pure Mode I study (Nakamara and Parks 1988). Subramanya *et al*. (2005) performed numerical investigation on the 3D elastic-plastic stress field near a crack front in a ductile material under mixed mode I-II loading using a boundary-layer small-scale yielding model of a thin plate. The approach used is similar to that by Nakamura and Parks (1988) but it includes a mixity ratio to introduce mixed mode fracture, by applying a remote elastic mixed mode stress, and results are presented for two values of the mixity ratio. Kotousov (2007), using first order plate theory, investigated the fracture in plates of finite thickness. Prawoto *et al*. (2009, 2011) employed two-dimensional and three-dimensional modeling using Abaqus to study compact tension specimen of multiphase material and concluded that the conditions at the crack front are key to fatigue performance. Shlyannikov and Tumnov (2011) investigated the stress fields and mode mixity for a surface semi-elliptical crack in a plate under biaxial loading. Sevcik *et al*. (2011) performed numerical calculations to study the effect of thickness on the crack front shape in a fatigue specimen.

Most of the studies undertaken so far are focused on pure Mode I, except Nakamura and Parks (1988) for pure Mode II and Subramanya *et al*. (2005) for mixed mode I-II. The study performed by Subramanya *et al*. (2005) employs a small-scale yield model and simulates a small circular disk around the crack front, while applying an assumed remote elastic plane stress state with mixed mode introduced through the mixity ratio parameter. This boundary-layer type approach has the disadvantage that the crack length *a* is unavailable as a characterizing parameter. In addition, the effect of thickness has not been studied explicitly in the literature; some available studies consider only fatigue loading. Therefore, in the present study, 3D effects at the crack front are explicitly

considered by studying complete mixed mode I-II single edge-notched tension (SENT) specimen. In addition, the effect of thickness on the stress field is studied for six different values of thickness, and the effect of mixed mode I-II is investigated for three values of crack inclination angle. Results on elastic analysis are presented to explore the extent of plane stress and plane strain conditions and to investigate the effect of thickness. The above results are obtained employing a 3D finite element model completely developed in ANSYS environment, including the meshing of the crack front using a novel technique introduced in this research work.

2. Problem setup

A single edge notched tension (SENT) specimen is considered in this study (Fig. 1). The SENT specimen is modified to accommodate mixed mode I-II, by varying crack inclination angle. The specimen width is W, the height is $2L$ and the thickness is B. The crack length is a, and β is the crack inclination angle measured from the loading axis ($\beta = 90^{\circ}$ implies pure Mode I loading). The numerical values used are $W = 50$ mm, $L = 100$ mm, $a = 10$ mm. Three values for the crack inclination angle β are considered: 90°, 70°, 50°. The thickness B of the specimen is varied as 1, 2, 4, 8, 16, and 32 mm.

2.1 Finite element model

The commercial finite element software ANSYS version 11 is used to perform a finite element analysis. The mixed mode I-II SENT specimen configuration as detailed above is built in ANSYS.

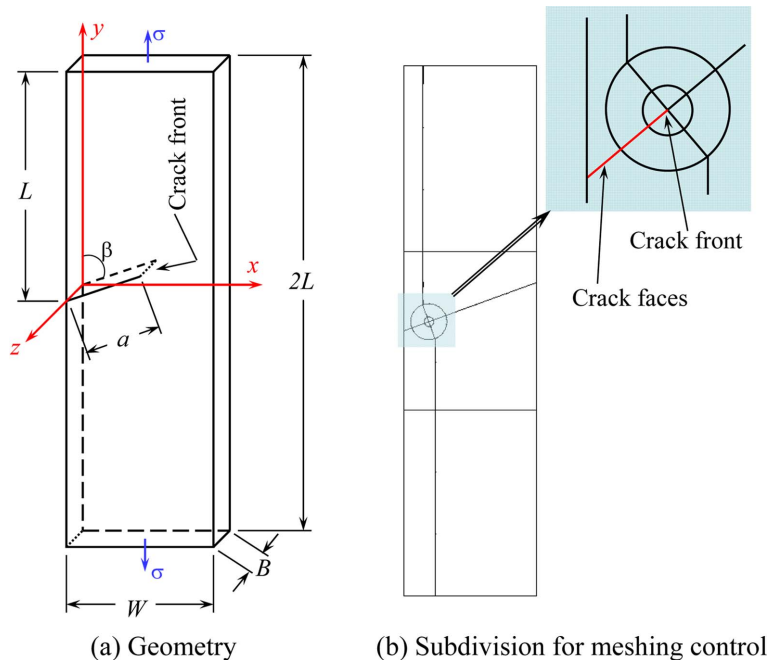(a) Geometry   (b) Subdivision for meshing control

Fig. 1 Mixed Mode I-II Single edge notched tension (SENT) specimen

The material behavior is assumed to be elastic isotropic with the following values of the elastic parameters: $E = 207$ GPa and $\nu = 0.3$. The meshing of a fracture mechanics model requires special attention to achieve the $1/\sqrt{r}$ stress singularity at the crack tip/front. As is well known, there are two main approaches. The first approach uses specialized crack tip/front finite elements, which contain the stress intensity factors as unknowns. There are two formulations that utilize this concept: the first formulation creates hybrid crack tip/front finite elements (Alturi *et al*. 1978, Pian and Moriya 1978), whereas the second formulation creates enriched crack tip/front finite elements (Benzley 1974, Gifford and Hilton 1978, Ayhan 2007). The difference between such two formulations lies in the implementation of the interelement displacement compatibility. The second approach utilizes standard parabolic (8-noded quadrilateral for 2D and 20-noded brick for 3D) finite elements, and generates singular finite elements by performing two steps. In the first step, an edge of the 8-noded quadrilateral element or a face of the 20-noded brick element is collapsed; in the second step, the midside nodes are placed at one quarter of the element size, from the collapsed edge or face. These triangular (2D) or wedge (3D) shaped singular finite elements around the crack tip/front with the collapsed edge or face at the crack tip/front generate the required $1/\sqrt{r}$ singularity. Such an approach is used in this study. ANSYS has a built-in function (KSCON) to perform the above-mentioned two steps for meshing the crack tip (2D), but it lacks such a function for meshing a crack front (3D). The first step of collapsing the face of a brick element can be easily performed in ANSYS. However, the meticulous job of placing collapsed wedge-shaped elements around the crack front with the collapsed face at the crack front must be done manually by the user, or expensive third-party crack-front meshing software must be used. In the present study, a novel technique is introduced to properly mesh the crack front using commands available in ANSYS, for mixed mode I-II SENT specimen. It is performed as follows. First, a two-dimensional geometrical model of the SENT specimen is generated with the crack being represented by two overlapping lines. The bottom-up technique as described in ANSYS manuals is used, and the specimen is subdivided into suitable size and shape regions to facilitate meshing. The typical subdivision used in the present study is shown in Fig. 1(b). Then, the KSCON command available in ANSYS is used to define singular finite elements' properties at the crack tip. This 2D model is meshed using non-solving four and eight noded finite elements, with eight noded finite elements restricted to the sub-regions close to the crack tip. The last step is to *extrude* the meshed 2D model to the required thickness and number of finite elements through the thickness. The finite element defined for the last step is the 20-node brick element.

To ensure correct dependence of stress on θ (polar coordinate), the mesh is highly refined around the crack front. The meshed model is shown in Fig. 2(a) with Fig. 2(b) and 2(c) showing the blown up crack front mesh for pure Mode I and mixed mode I-II respectively. Taking advantage of symmetry through thickness, only a half of the specimen is modeled, using symmetric boundary conditions on the mid plane ($z = 0$). The lower face, $y = -L$, is fixed in all degrees of freedom to prevent rigid body motion. A uniaxial stress equal to 20 MPa is applied at the upper face ($y = L$) of the specimen.

2.2 Mesh sensitivity analysis

A mesh sensitivity analysis is performed to ensure optimum mesh size for proper convergence and accurate numerical results. The value of maximum von Mises stress ($\sigma_{\text{Mises, max}}$) occurring in the model is used as the convergence criterion, and the case of a pure Mode I crack ($\beta = 90^{\circ}$) is

(a) Complete model

(b) Crack front mesh (Mode I) (crack shown by thick line)

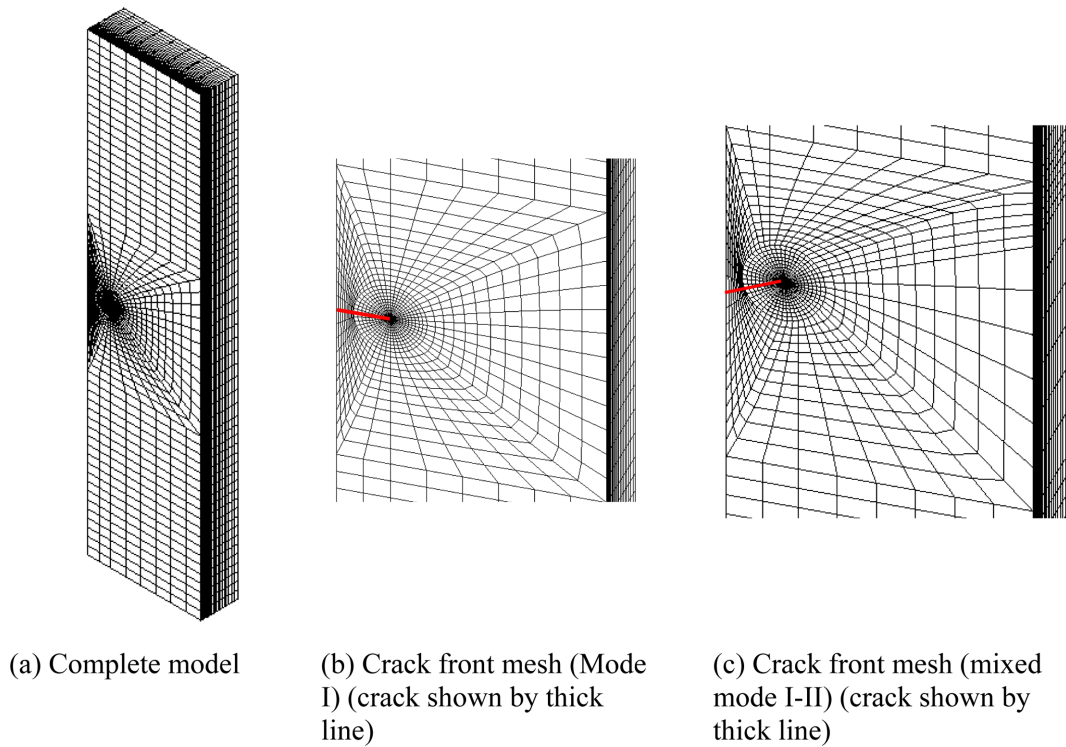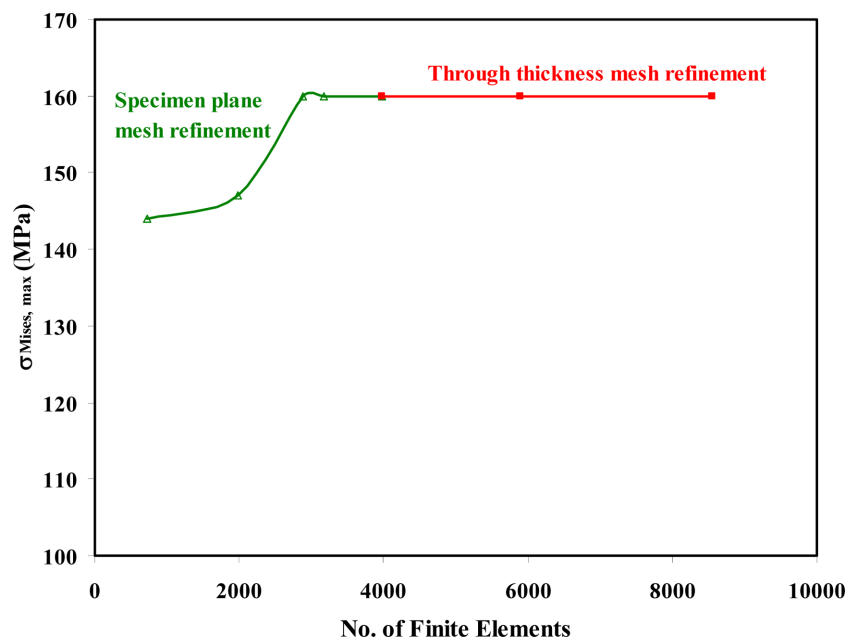(c) Crack front mesh (mixed mode I-II) (crack shown by thick line)

Fig. 2 Meshed finite element model

Fig. 3 Mesh sensitivity analysis; $\beta = 90^{\circ}$

employed. The mesh is refined in two steps: in the first step, it is refined only in the plane of the SENT specimen (xy-plane). Once the mesh is optimal in the specimen plane, the mesh is then refined through the thickness. Finite elements of varying thicknesses are used through the thickness of the specimen, where the layers of finite elements become thinner towards the free surface. Results are shown in Fig. 3. Starting with 720 finite elements, the mesh is first refined in the plane of the specimen up to 3984 elements (at this stage the mesh is optimized in the plane of the specimen). Then the mesh is refined in the thickness direction up to 8544 finite elements (at this stage the mesh is completely optimized). The optimized mesh is shown in Fig. 2.

3. Results and discussion

3.1 Effect of the thickness

Fig. 4 shows the von Mises stress curves at the crack front for six thicknesses under pure Mode I loading ($\beta = 90°$). The stress values plotted in Fig. 4 (and Figs. 5, 6, 7 and 9) are interpolated along a straight defined path. This defined path, for example for Fig. 4, is the distance from the crack front in x-direction, plotted on abscissa after normalizing by the crack length a. Fig. 4(a) shows the results at the outer free surface ($z = 0.495B$), whereas Fig. 4(b) shows the results at the mid plane of specimen ($z = 0.005B$). For both the cases, theoretical solutions for crack-tip stresses for both plane stress and plane strain conditions are also plotted for comparison. At the free surface ($z = 0.495B$), there is a little variation in the stress fields with increasing thickness. The near crack-front stress values are close to the theoretical plane stress solution and eventually coincide with it at some distance away from the crack front. At the mid plane ($z = 0.005B$), the near crack front stresses quickly shift towards the theoretical plane strain solution as the thickness is increased. This shows the development of plane strain zone near the crack front at the mid plane of the specimen. In this case too, the stresses coincide with the theoretical plane stress solution away from the crack front. The results shown in Figs. 4(a) and 4(b) confirm, with increasing thickness, the transition from plane stress to plane strain state deep inside the specimen, while plane stress state prevails at the free surface as is shown by Jendoubi *et al*. (1991). These results validate the present numerical model.

Fig. 5 shows the variation of $\sigma_{zz}/\nu(\sigma_{xx} + \sigma_{yy})$ along the normalized distance at the crack front for six values of thickness. Fig. 5(a) plots the variation at the free surface ($z = 0.495B$) showing that a triaxial stress state exists up to a short distance ($0.15a$), whereas the stress state is purely plane stress after this point. The specimen thickness affects only the magnitude of the triaxial stress and has no effect on the extent of this triaxial stress state. Fig. 5(b) plots the variation at the mid plane ($z = 0.005B$) predicting a strong dependence on the thickness. With increasing thickness, the stress state at the crack front shifts towards pure plane strain ($\sigma_{zz}/\nu(\sigma_{xx} + \sigma_{yy}) \rightarrow 1$), whereas the extent of the triaxial stress state at the crack front (the distance from the crack front where $\sigma_{zz} = 0$) increases.

Fig. 6 shows the variation of $\sigma_{zz}/\nu(\sigma_{xx} + \sigma_{yy})$ through the thickness along the crack front. While the stress state at the free surface is always plane stress, triaxial stress state exists through the thickness. The plane strain condition is achieved first at the specimen mid plane and the extent of it towards the free surface increases with increasing the thickness. Based on an experimental study using strain gauges, Ranganathan *et al*. (1994) analyzed three thicknesses and found that 4 mm thick samples showed plane stress state, while 12 and 30 mm thick samples showed plane strain
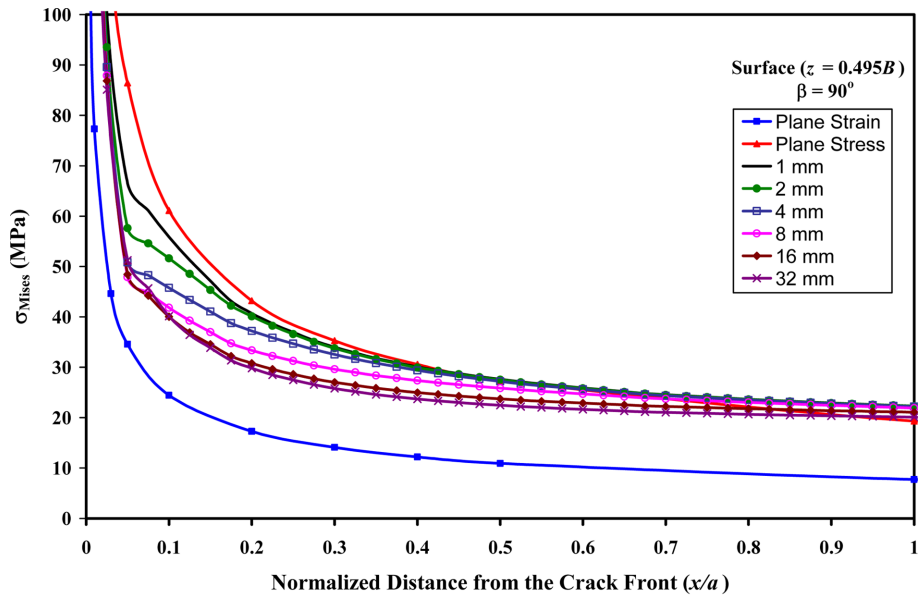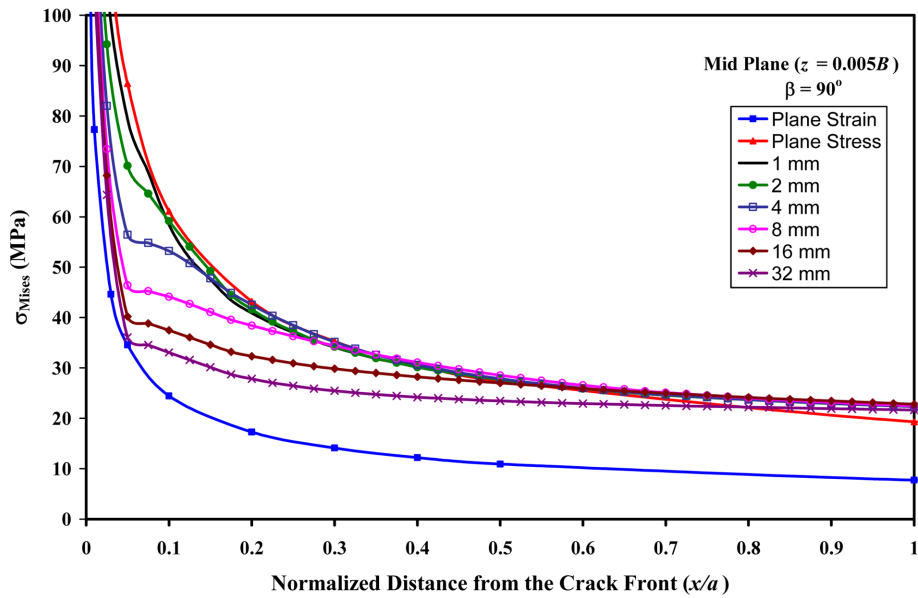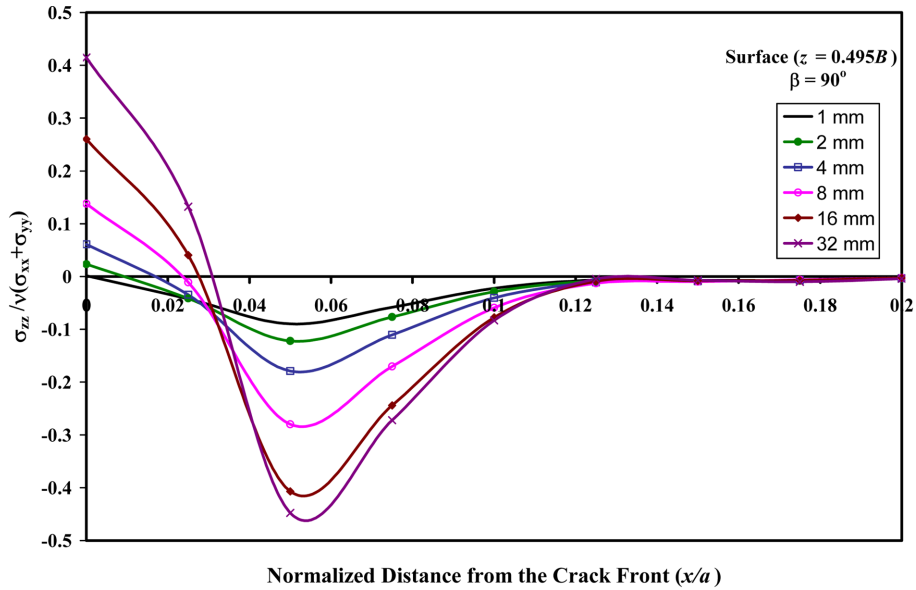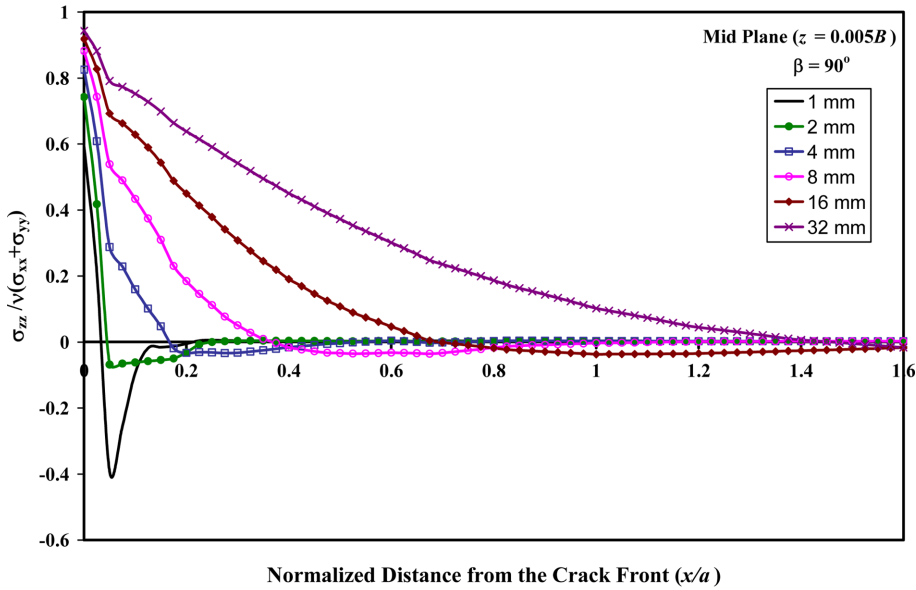
(a) at surface for $\beta = 90^{o}$

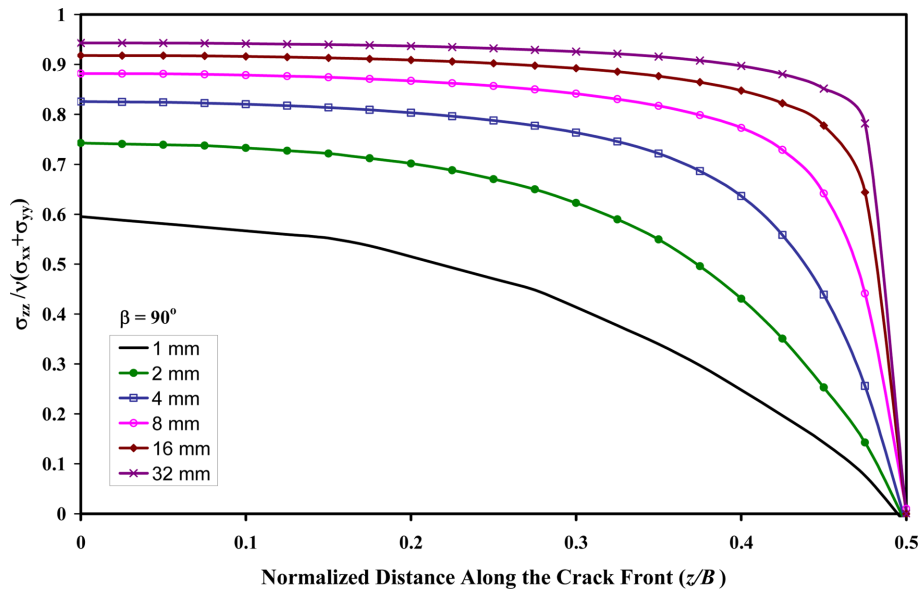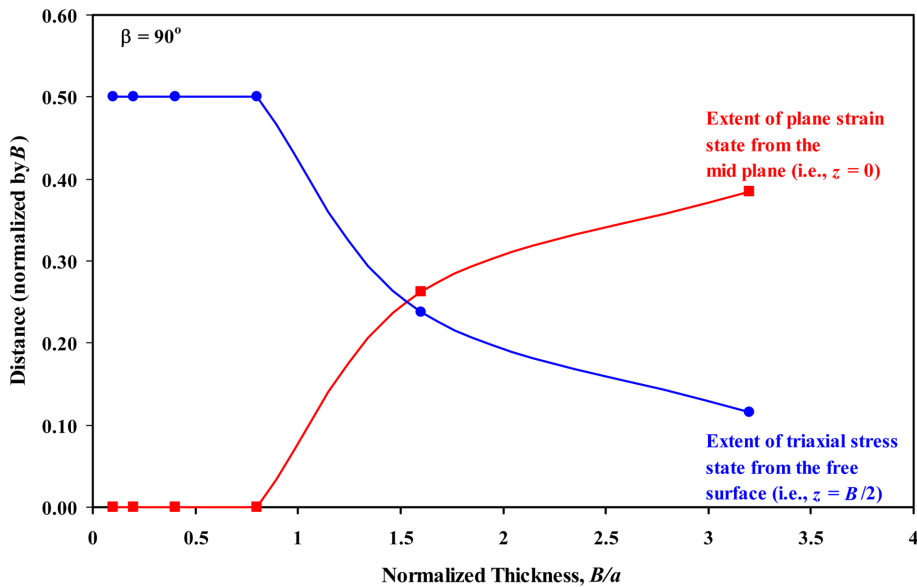(b) at mid plane for $\beta = 90^{o}$

Fig. 4 Effect of the thickness: von Mises stress at the crack front

behavior at the crack front. The present study agrees with the above experimental study.

Fig. 7 presents the dependence of the stress state at the crack front on the thickness. The abscissa represents the thickness normalized by the crack length a, whereas the ordinate shows respective distance normalized by the thickness B. The two curves show the two distances, namely the extent

(a) at surface for $\beta = 90^o$

(b) at mid plane for $\beta = 90^o$

Fig. 5 Effect of the thickness: normalized σ_{zz} at the crack front

of triaxial stress state from the free surface (i.e., $z = B/2$) towards the mid plane and the extent of plane strain state from the mid plane (i.e., $z = 0$) towards the free surface, each normalized by the thickness B. Both the curves are extracted from Fig. 6 and $\sigma_{zz}/\nu(\sigma_{xx} + \sigma_{yy}) > 0.9$ is used as the criterion for the plane strain state. Only the triaxial stress state exists throughout the thickness up to

Fig. 6 Variation of normalized σ_{zz} through thickness; $\beta = 90^{\circ}$

Fig. 7 Variation of the extent of stress states at the crack front with thickness; $\beta = 90^{\circ}$

a ratio of $B/a = 0.8$ and plane stress state is non-existent. For $B/a > 0.8$, plane strain condition appears at the mid-plane, and shows steady increase towards the free surface. Approximately at $B/a = 1.5$, the transition from predominantly triaxial stress to plane strain state occurs in the thickness and the extent of plane strain state continues to increase. The plain strain state is not expected to

completely dominate (i.e., reaching a value of 0.5 on ordinate in Fig. 7) the thickness as the plane stress state always exists at the free surface and there must be a transitional triaxial stress state between the two stress states.

Fig. 8 presents the development of the plane strain zone with increasing thickness for pure Mode I crack. The $\sigma_{zz}/\nu(\sigma_{xx} + \sigma_{yy})$ contours are shown on the yz-plane at $x = a$ for four values of thickness. In all cases, the crack front lies at the center of each contour plot in the plane of the figures (shown by thick red lines) and the crack faces lie normal to the plane of the figures. By comparing Fig. 8 with Fig. 6, these contour plots provide an insight into the development of the plane strain zone and its evolution with increasing the thickness.

3.2 Effect of the crack inclination angle

Fig. 9 represents the variation of $\sigma_{zz}/\nu(\sigma_{xx} + \sigma_{yy})$ through the thickness and along the crack front for three values of thickness, and three values of crack inclination angle. The values of crack inclination angle β used in addition to 90°, are 70° and 50°, which are moderate to strong Mode II
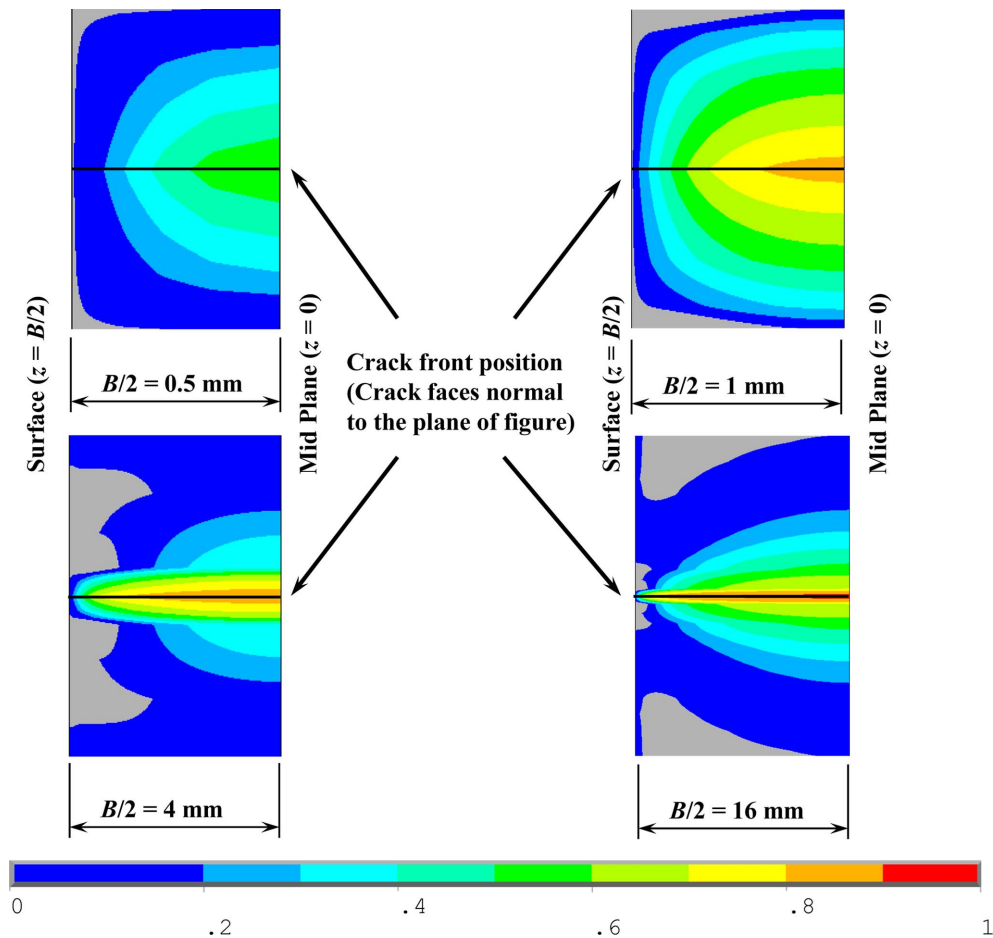

Fig. 8 Development of plane strain zone with thickness; $\beta = 90^\circ$, $\sigma_{zz}/\nu(\sigma_{xx} + \sigma_{yy})$ contours shown
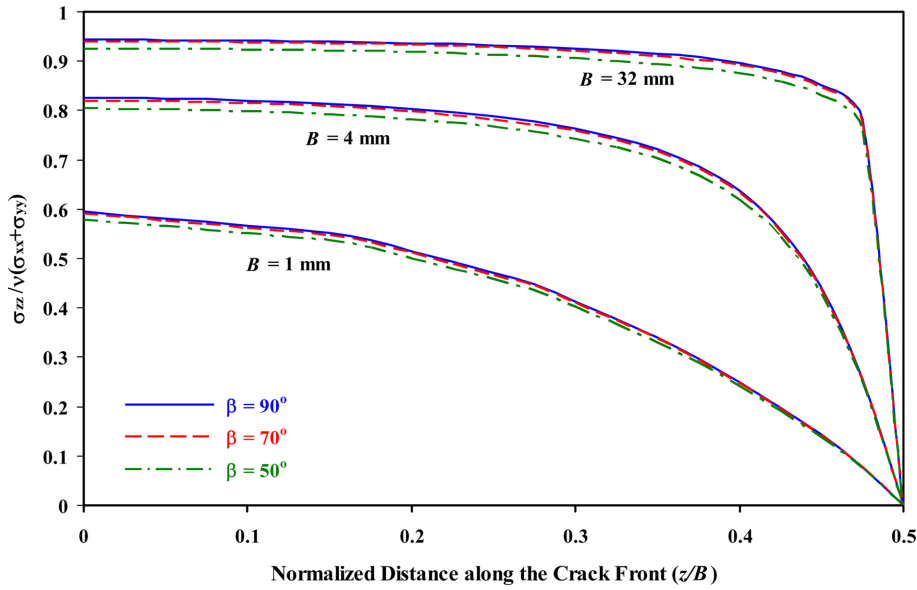
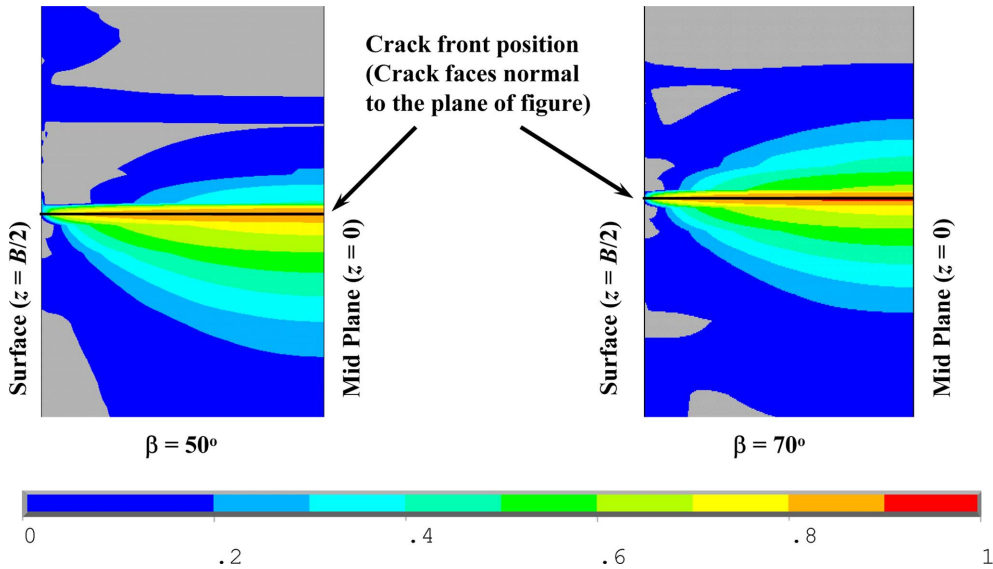Fig. 9 Variation of normalized σ_{zz} through thickness: effect of different crack inclination angles

Fig. 10 $\sigma_{zz}/\nu(\sigma_{xx} + \sigma_{yy})$ contours for $\beta = 50^{\circ}$ and 70°, $B/2 = 16$ mm

configurations. As observed, the effect of mixed mode I-II on the triaxial stress state at the crack front is negligible as compared to pure Mode I results. Therefore, the results in Fig. 7 can safely be extended to mixed mode I-II for $\beta > 45^{\circ}$.

Fig. 10 represents the $\sigma_{zz}/\nu(\sigma_{xx} + \sigma_{yy})$ contours for $\beta = 70^{\circ}$ and 50° for thickness $B/2 = 16$ mm, similar to those plotted in Fig. 8 for pure Mode I. A comparison of these results with those in Fig. 8 (for $\beta = 90^{\circ}$ and thickness $B/2 = 16$ mm) shows a deviation from symmetry about the crack front.

This unsymmetric distribution of the $\sigma_{zz}/\nu(\sigma_{xx} + \sigma_{yy})$ contours is analogous to the observed behavior of various quantities (strain energy, Mises stress etc) plotted at the crack tip in two-dimensions (Theocaris and Andrianopoulos 1982, Khan and Khraisheh 2004). The degree of deviation from symmetric behavior increases with decreases crack inclination angle (implying increasing mode II effect). Such contours provide an insight and understanding of 3D stress states.

4. Conclusions

1. The effect of the thickness is explicitly investigated using a modified mixed mode SENT specimen for both pure Mode I and mixed mode I-II cracks.

2. At the surface, the thickness affects only the magnitude of the triaxial stress, whereas it affects both the magnitude and extent of the triaxial stress at the mid plane of the specimen (Fig. 5).

3. The extent of various stress states along the crack front is correlated to thickness. It is found that the transition from predominantly triaxial stress to predominantly plain strain state occurs at $B/a = 1.5$ (Fig. 7).

4. $\sigma_{zz}/\nu(\sigma_{xx} + \sigma_{yy})$ contours at the crack front are presented for both pure Mode-I and mixed mode I-II, which provide an insight of the development of various stress states at the crack front.

5. Results for the stress state at the crack front for mixed mode I-II cracks are presented for two crack inclination angles, and results compared with pure Mode I. It is found that the effect of mixed mode on the triaxial stress, as compared to pure Mode I, is very small (Fig. 9).

6. A novel technique is introduced to mesh the crack front (3D) with singular finite elements using commands available in ANSYS environment without the need for third-party software.

Acknowledgements

References

Alturi, S.N., Nakagaki, M., Kathiresan, K., Rhee, H.C. and Chen, W.H. (1978), "Hybrid finite element models for linear and nonlinear fracture analysis", *Proceedings of the International Conference on Numerical Methods in Fracture Mechanics*, Ed. Owen, D.R.J., editor. Swansea, UK.

Ayhan, A.O. (2007) "Mixed mode stress intensity factors for deflected and inclined corner cracks in finite-thickness plates", *Int. J. Fatigue*, **29**, 305-317.

Banks, T.M. and Garlick, A. (1984), "The form of crack tip plastic zones", *Eng. Frac. Mech.*, **19**(3), 571-581.

Benzley, S.E. (1974) "Representation of singularities with isoparametric finite elements", *Int. J. Numer. Meth. Eng.*, **8**, 537-545.

Gifford, Jr. L.N. and Hilton, P.D. (1978), "Stress intensity factors by enriched finite elements", *Eng. Frac. Mech.*, **10**, 485-496.

Jendoubi, K., Ranganathan, N. and Merah, N. (1991), "Effect of thickness on elasto-plastic deformation and hysteretic energy dissipated at crack tip", *J. Test. Eval.*, **19**(3), 201-209.

Khan, S.M.A. Khraisheh, M.K. (2004), "A new criterion for mixed mode fracture initiation based on the crack tip plastic core region", *Int. J. Plasticity*, **20**, 55-84.

Kim, K., Kim, K. and Shim, C. (2003), "A study on the measurement of plastic zone and crack growth length at the crack tip under cyclic loading using ESPI system", *Struct. Eng. Mech.*, **15**, 367-378.

Kotousov, A. (2007), "Fracture in plates of finite thickness", *Int. J. Solids Struct.,* **44**, 8259-8273.

Maccagno, T.M. and Knott, J.F. (1989), "The fracture behavior of PMMA in mixed modes I and II", *Eng. Frac. Mech.*, **34**(1), 65-86.

Mishra, S.C. and Parida, B.K. (1985), "Determination of the size of crack-tip plastic zone in a thin sheet under uniaxial loading", *Eng. Frac. Mech.*, **22**(3), 351-357.

Nakamura, T. and Parks, D.M. (1988), "Three-dimensional stress field near the crack front of a thin elastic plate", *J. Appl. Mech.*, **55**, 805-813.

Nakamura, T. and Parks, D.M. (1989), "Antisymmetrical 3D stress field near the crack front of a thin elastic plate", *Int. J. Solids Struct.*, **25**(12), 1411-1426.

Pian, T.H.H. and Moriya, K. (1978), "Three dimensional fracture analysis by assumed stress hybrid elements", *Proceedings of the International Conference on Numerical Methods in Fracture Mechanics*, Ed. Owen, D.R.J., Swansea, UK.

Prawoto, Y., Idris, R., Kamsah, N. and Tamin, N. (2009), "Two-dimensional modeling to compute plastic zone in front of compact tension sample of a multiphase material", *Comput. Mater. Sci.*, **47**, 482-490.

Prawoto, Y., Idris, R., Kamsah, N. and Tamin, N. (2011), "Three-dimensional modeling to compute plastic zone in front of crack in compact tension sample of multiphase material", *Comput. Mater. Sci.*, **50**, 1499-1503.

Ranganathan, N., Jendoubi, K. and Merah, N. (1994), "Experimental characterization of the elastic-plastic strain fields at the crack tip due to cyclic loading", *J. Eng. Mat. Tech.*, **116**, 187-192.

Sevcik, M., Hutar, P., Zouhar, M. and Nahlik, L. (2011), "Numerical estimation of the fatigue crack front shape for a specimen with finite thickness", *Int. J. Fracture*. (in press)

Shlyannikov, V.N. and Tumnov, A.V. (2011), "Mixed mode 3D stress fields and crack front singularities for surface flaw", *Procedia Eng.*, **10**, 1133-1138.

Subramanya, H.Y., Viswanath, S. and Narasimhan, R. (2005), "A three-dimensional numerical study of mixed mode (I and II) crack tip fields in elastic-plastic solids", *Int. J. Frac.*, **136**, 167-185.

Theocaris, P.S. and Andrianopoulos, N.P. (1982), "The Mises elastic-plastic boundary as the core region in fracture criteria", *Eng. Frac. Mech.*, **16**(3), 425-432.

Wang, J., Guo, W.L. and Shen, Y.P. (1996), "The shape and size of crack tip plastic zones under triaxial stress constraint", *Int. J. Frac.*, **80**, R61-R68.